20231025

Experimental Consideration on Mode Electricity Consumption of Permanent Magnet Synchronous Motor with Torque Ripple Suppression Control Considering Magnetic Saturation

Taiki Mikami*, Keitaro Kawarazaki†, Nobukazu Hoshi‡

Tokyo University of Science, Dept. of Electrical Engineering, Faculty of Science and Technologies, Tokyo, Japan
*E-mail: *mikdora007@icloud.com, †kawaratheki@gmail.com, ‡nhoshi@rs.tus.ac.jp*

ABSTRACT: Torque ripple in permanent magnet synchronous motors can be suppressed using various methods, including torque ripple suppression control, which considers magnetic saturation and can suppress torque ripple over a wide operating range. However, the impact of this method on efficiency under variable speed drive has not been thoroughly investigated. Therefore, this paper verified the effect of torque ripple suppression control considering magnetic saturation on efficiency by creating efficiency maps and experimentally deriving losses under variable speed drive in an electric vehicle driving mode. The results show that the increase in loss under driving with torque ripple suppression control was approximately 0.2% compared to without, which had little effect on electricity consumption reduction.

KEY WORDS: Torque ripple suppression, interior permanent magnet synchronous motor, electric vehicle, WLTC mode, electricity consumption.

1. INTRODUCTION

Electric vehicles (EVs) are one promising solution for reducing carbon dioxide emissions and dependence on fossil fuels. However, achieving optimal driving performance and comfort is important for EVs to spread further. Permanent magnet synchronous motors (PMSMs) are often used as electric vehicle traction motors. Torque ripple, a common issue in PMSMs, can negatively impact vehicle stability, comfort, and efficiency. Therefore, it is important to develop effective methods for suppressing torque ripple and improving driving performance of EVs.

Several methods for torque ripple suppression have been proposed. One method is using a torque meter to measure and suppress torque ripple [(1)]. However, this method is expensive due to the cost of the torque meter and requires considering the torque meter bandwidth. Another method estimates torque by linearly approximating the current–flux linkage characteristics (hereafter referred to as magnetization characteristics) of a motor from a mathematical model [(2)–(6)]. However, this method does not consider nonlinearities such as magnetic saturation or cross-coupling, and torque ripple suppression is difficult under high torque ranges where magnetic saturation is noticeable. To solve this problem, a torque ripple suppression method that considers nonlinearities by modeling spatial harmonics components of flux linkage has been proposed [(7)]. According to reference (7), torque ripple can be suppressed under high torque ranges, and it has been shown that 6th-order torque ripple can be suppressed by up to 69.1%. References (8) and (9) have shown that efficiency declines by flowing current that can suppress torque ripple. However, the influence of torque ripple suppression on efficiency under variable speed drive has not been considered.

This paper verifies the influence of torque ripple suppression control proposed in reference (7) on efficiency with multiple operating points. And variable speed drive test was conducted using a driving pattern that simulates EV driving on a motor bench. The influence of torque ripple suppression control considering magnetic saturation on loss was verified by comparing a loss with and without torque ripple suppression control.

2. TORQUE RIPPLE SUPPRESSION CONTROL METHOD

In this chapter, the torque ripple suppression method proposed in reference (7) that uses a torque estimation equation considering the nonlinearity of magnetization characteristics is explained, and a constraint on the motor rotational speed that can suppress torque ripple is derived.

2.1. Torque ripple estimation equation

In reference (7), the torque ripple is suppressed by generating q-axis compensation current command i^*_{qh} [A] using the estimated torque ripple $\hat{T}_{\mathrm{h}}$ [Nm] and superimposing it on the q-axis current command. The following equation expresses the estimated torque ripple that considers the nonlinearity of magnetization characteristics.

$$\hat{T_{\mathrm{h}}}(i_{\mathrm{d}}, i_{\mathrm{q}}, \theta) = P\left\{\sum_{k=1}^{k_{\max}} 6k\Big(W'_{\mathrm{qs}6k}\cos 6k\theta - W'_{\mathrm{qc}6k}\sin 6k\theta + W'_{\mathrm{ds}6k}\cos 6k\theta - W'_{\mathrm{dc}6k}\sin 6k\theta\Big)\right\}, \quad (1)$$

where $\hat{T}_{\mathrm{h}}(i_{\mathrm{d}}, i_{\mathrm{q}}, \theta)$ is the estimated torque ripple [Nm], P is the number of pole pairs, k = 1,2,3,$\cdots$, W' are 6th-order sine and cosine coefficients of magnetic co-energy, θ is the angle of the d-axis in synchronous rotation coordinate system with respect to U phase [rad]. The following equation can obtain the 6th-order sine and cosine coefficients of the magnetic co-energy.

$$\begin{cases} W'_{\mathrm{qc}6k} = \int_0^{i_{\mathrm{q}}} \lambda_{\mathrm{qc}6k}(0, i'_{\mathrm{q}}) di'_{\mathrm{q}} \\ W'_{\mathrm{qs}6k} = \int_0^{i_{\mathrm{q}}} \lambda_{\mathrm{qs}6k}(0, i'_{\mathrm{q}}) di'_{\mathrm{q}} \\ W'_{\mathrm{dc}6k} = \int_0^{i_{\mathrm{d}}} \lambda_{\mathrm{dc}6k}(i'_{\mathrm{d}}, i_q) di'_{\mathrm{d}} \\ W'_{\mathrm{ds}6k} = \int_0^{i_{\mathrm{d}}} \lambda_{\mathrm{ds}6k}(i'_{\mathrm{d}}, i_q) di'_{\mathrm{d}} \end{cases}, \tag{2}$$

where $\lambda_{\mathrm{qc}6k}(0, i'_q), \lambda_{\mathrm{qs}6k}(0, i'_{\mathrm{q}}), \lambda_{\mathrm{dc}6k}(i'_d, i_{\mathrm{q}}), \lambda_{\mathrm{ds}6k}(i'_{\mathrm{d}}, i_{\mathrm{q}})$ are magnetization characteristics of spatial harmonics components [Wb], $i'_{\mathrm{d}}, i'_{\mathrm{q}}$ are the intermediate variable in the definite integral. The current integrals of these λ are calculated by dividing the integration interval [0, i] into $N = \frac{i}{\Delta i}$ sections of every tick width $\Delta i = (i_{\mathrm{n+1}} - i_{\mathrm{n}})$ and integrating trapezoidally with a linear approximation of the magnetization characteristics of each section, as shown in Fig. 1. The magnetization characteristics are obtained using the estimation method of harmonics components of flux linkage proposed in reference (7). Note that when $i_{\mathrm{d}} = 0$ control is applied, magnetic co-energy should be considered only the q-axis one since the definite integral for the d-axis current is zero.

The q-axis compensation current command i^*_{qh} is expressed by the following equation.

$$i^*_{\mathrm{qh}} = \frac{-\hat{T}_{\mathrm{h}}}{P\{(L_{\mathrm{d}} - L_{\mathrm{q}})i_{\mathrm{d}} + \Psi_{\mathrm{a}}\}}, \tag{3}$$

where L_{d} is d-axis inductance [H], L_{q} is q-axis inductance [H], i_{d} is d-axis current [A], and Ψ_{a} is permanent magnet flux linkage [Wb]. The q-axis compensation current command is obtained by substituting the estimated torque ripple calculated by (1) into (3). The $6k$th-order torque ripple can be suppressed by superimposing this q-axis compensation current command on the q-axis current command. Note that the experiment only considered 6th-order torque ripple in this research.

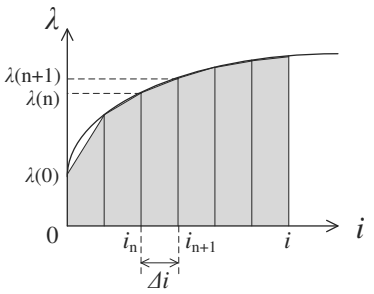

Fig. 1 Calculation of magnetic co-energy.

2.2. Applicable range of torque ripple suppression control

When superimposing 6th-order harmonic currents on the current command to suppress torque ripple, the 6th-order harmonic components are attenuated above the cutoff frequency of the transfer function of the current control system [10]. Therefore, the closed-loop transfer function of the current control system is derived here to obtain the upper limit of the rotational speed at which the 6th harmonic current can be superimposed. The closed-loop transfer function of the current controller is expressed as

$$G(s) = \frac{K_{\mathrm{P}} s + K_{\mathrm{I}}}{Ls^2 + (R_{\mathrm{a}} + K_{\mathrm{P}})s + K_{\mathrm{I}}}, \tag{4}$$

where K_{P} and K_{I} are the proportinal and integral gains of the current control system, respectively, L [H] is d- or q-axis inductance, and R_{a} [Ω] is winding resistance. Assuming that the cutoff angular frequency in (4) is ω_{c} [rad/s], the condition for being able to flow the 6th harmonic current without attenuation is as follows.

$$\omega_{\mathrm{m}} \leq \frac{\omega_{\mathrm{c}}}{6P}, \tag{5}$$

where ω_{m} [rad/s] is the angular velocity in mechanical angle. The motor parameters are shown in Table 1, and the proportional and integral gains of the current controller are set to 0.995 and 76.78, respectively. Under these conditions, the closed-loop transfer function from the PI controller to the motor, shown in (4), was calculated in (5) using the values in Table 1. As a result, the maximum rotational speed at which the 6th harmonic current does not attenuate is 400 min^{-1}.

3. EXPERIMENT

This chapter discusses the system configuration of the motor test bench used in this experiment and the efficiency with and without torque ripple suppression control during $i_{\mathrm{d}} = 0$ control. The efficiency differences between the two are shown as efficiency maps.

Table 1 Parameters of experimental system.

Tested motor (IPMSM)	Rated power	44.5 kW
	Rated torque	175.0 Nm
	Rated speed	5000 min^{-1}
	Number of pole pairs	8
	Number of stator slot	24
	d-axis inductance L_{d}	428.9 μH
	q-axis inductance L_{q}	497.7 μH
	Permanent magnet flux linkage Ψ_{a}	74.5 mWb
	Winding resistance R_{a}	38.4 mΩ
Inverter	Carrier frequency	20 kHz
	DC voltage	360 V
Vehicle model	Sprung mass	800 kg
	Wheel radius	400 mm
	Gear ratio	2.60
Controller	Control cycle	25 μs

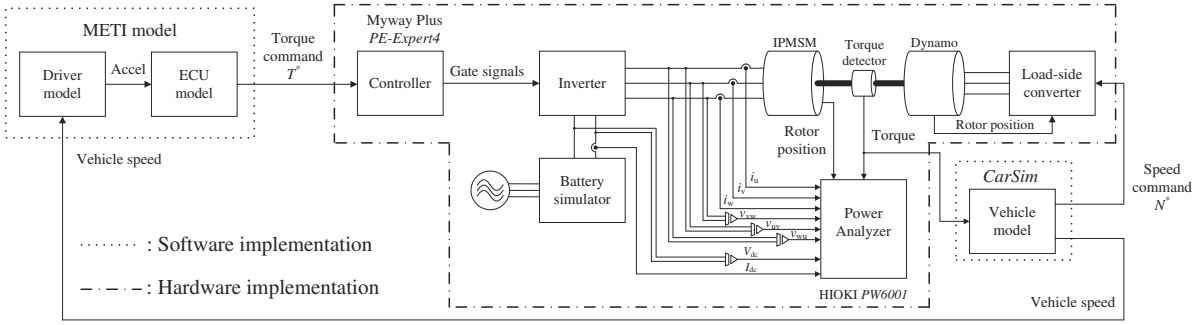

Fig. 2 Experimental system configuration.

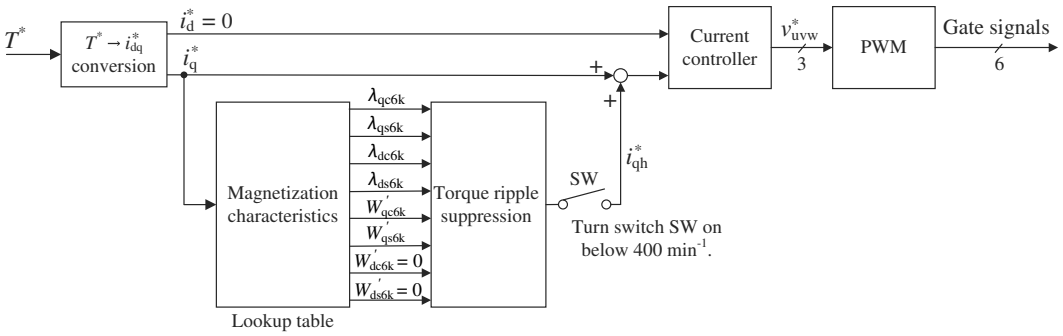

Fig. 3 Block diagram of the torque ripple suppression control used in this paper.

Furthermore, the variable speed drive test was conducted using WLTC mode, an EV driving test pattern. The influence of the torque ripple suppression control considering magnetic saturation on efficiency under variable speed drive is verified by comparing total losses with and without torque ripple suppression control.

3.1. Experimental system and conditions

Fig. 2 shows the experimental system configuration of the motor test bench used in this research. Torque control was conducted with an IPMSM, while rotational speed control was conducted with the load-side generator. A battery simulator maintained the inverter input voltage at 360 V. The gate signals of the inverter were generated by a controller, *PE-Expert4*, which also implemented the torque ripple suppression control.

In the variable speed drive test, the driver model was given the urban driving mode (Low) of the WLTC mode as the vehicle speed command. Accelerator position is determined by the difference between this vehicle speed command and the current vehicle speed calculated in the vehicle model, and the torque command is determined from the lookup table written in the ECU model. The vehicle model included parameters such as vehicle mass and gear ratio. Table 1 shows representative vehicle parameters in the vehicle model.

Fig. 3 shows the block diagram of the torque ripple suppression control implemented in *PE-Expert4*. The dq-axis current commands are generated based on $i_d = 0$ control for the torque command determined by the ECU model. The q-axis compensation current command i_{qh}^* that cancels the 6th-order harmonic component is generated using the magnetization characteristics table according to the generated q-axis current command. The switch SW in Fig. 3 determines whether i_{qh}^* is superimposed on the q-axis current command i_q. In this research, the switch SW is turned on below 400 min^{-1} to superimpose i_{qh}^* and suppress the torque ripple. The uvw-phase voltage commands v_{uvw}^* are generated by the dq-axis current controller with PI control.

3.2. Efficiency maps

Reference (7) reports that torque ripple suppression control has little effect on efficiency. However, reference (8) reports copper and iron losses increase due to superimposed harmonic current. This section verifies the influence of torque ripple suppression control on efficiency by creating the efficiency map. Fig. 4 shows a color map of the efficiency from the inverter input to motor output under $i_d = 0$ control. The efficiency map was created using the measured values of total efficiency, which were ob-

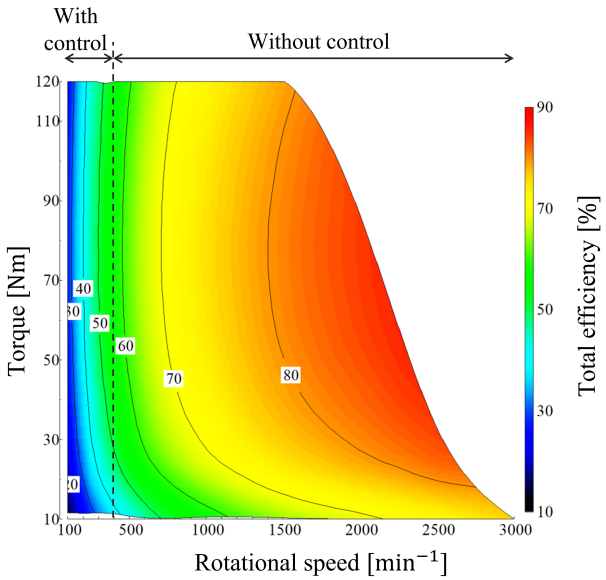

Fig. 4 Total efficiency map considering switching torque ripple suppression control.

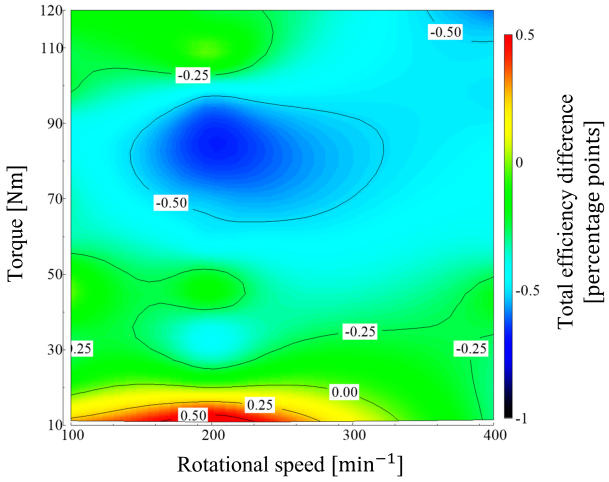

Fig. 5 Efficiency difference between with and without torque ripple suppression control ($\eta_r - \eta$).

tained by commanding the q-axis current commands from 20 to 240 A in 20 A increments at rotational speeds of 100, 200, 400, 500, 1000, 1500, 2000, 2500, and 3000 min^{-1}. However, data during torque ripple suppression control is used only at rotational speeds of 100, 200, and 400 min^{-1}, while data without torque ripple suppression control is used at other rotational speeds.

Fig. 5 shows a color map of the difference in efficiency (total efficiency with torque ripple suppression control η_r [%] minus without torque ripple suppression control η [%]). This figure shows that total efficiency is declining in most operating ranges. One of the reasons for the efficiency decline with torque ripple suppression control is the increase in copper loss. Fig. 6 shows

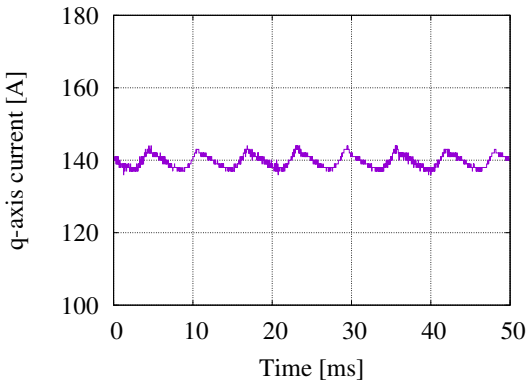

(a) Without torque ripple suppression.

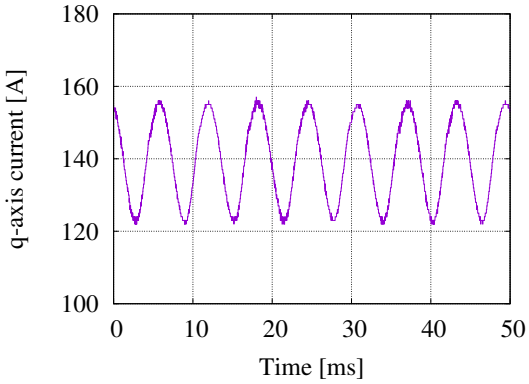

(b) With torque ripple suppression.

Fig. 6 Waveforms of the q-axis current (N_{ref} = 200 min^{-1}, T_{ref} = 80 Nm).

the q-axis current waveform at the motor rotational speed command of 200 min^{-1} and torque command of 80 Nm. With this method, copper loss of current harmonics increases due to superimposing the q-axis current harmonics that cancel the torque ripple compared to without torque ripple suppression control.

3.3. Variable speed drive test using the EV-driving mode

This section discusses the influence of torque ripple suppression control on electricity consumption during variable speed drive using the urban driving phase (Low) of WLTC driving mode. The maximum and minimum torque are set to 128 Nm and −100 Nm, respectively, with the upper motor rotational speed limited to 1000 min^{-1} to emphasize the influence of torque ripple suppression control on efficiency. To apply the torque ripple suppression control below 400 min^{-1}, the upper-speed limit was set at 1000 min^{-1} so that 400 min^{-1} is commanded more often. Note that parameters used in variable speed drive are shown in Table 1.

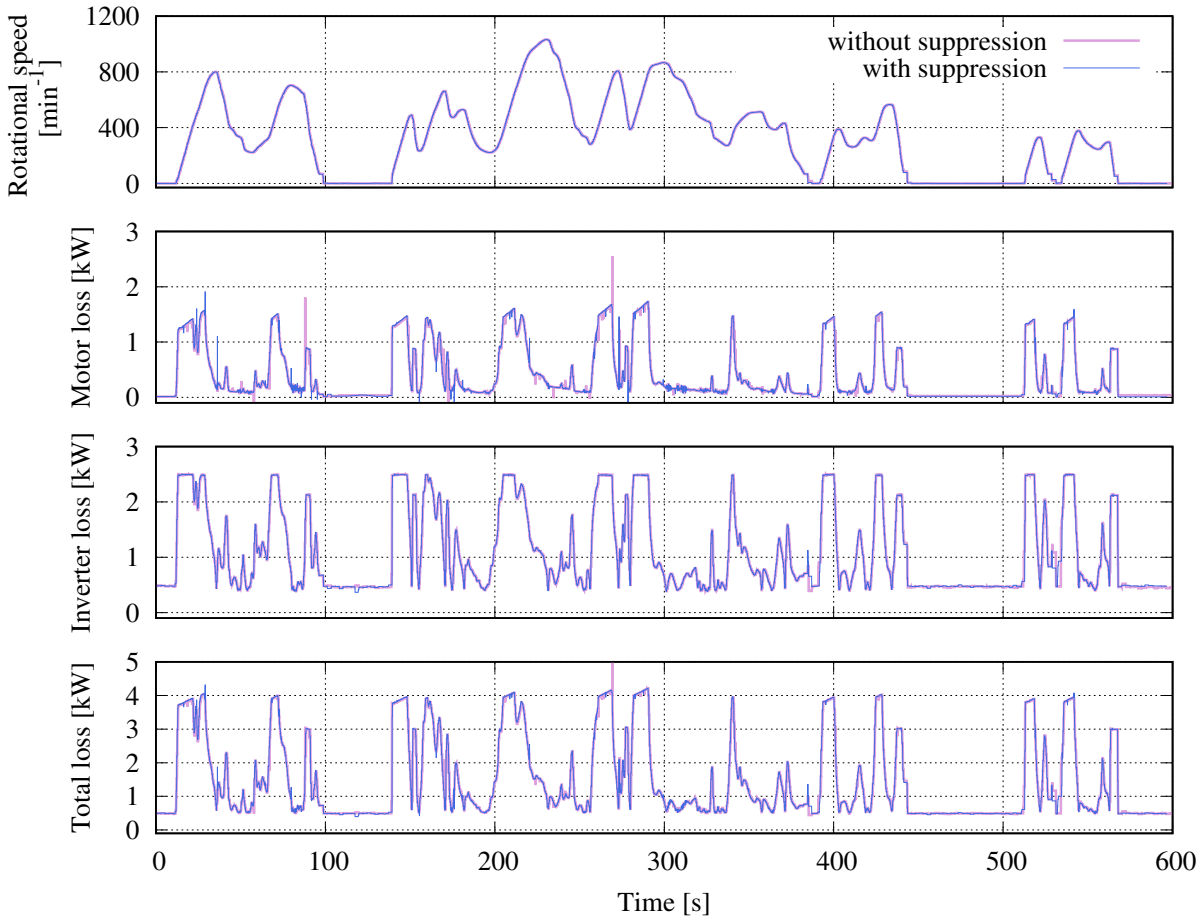

Fig. 7 Loss comparison under variable speed drive (with and without torque ripple suppression control).

3.3.1. Loss comparison between with and without torque ripple suppression control

Fig. 7 shows the motor rotational speed and losses during the urban driving phase of WLTC. Total loss refers to the loss from inverter input power to motor mechanical output. The characteristics of each loss in Fig. 7 are parallel to the horizontal axis near the apex of the graph, indicating that copper loss remains constant at these operating conditions, which correspond to a torque of 128 Nm, a limit value. However, the current vehicle speed calculated by the vehicle model is delayed relative to the vehicle speed command, which can cause spikes in losses, as shown in Fig. 7, due to torsional vibration.

The results indicate that total loss with and without torque ripple suppression control under low-phase driving is 876, and 874 kJ, respectively. Total loss increases, especially in high torque ranges above 80 Nm with torque ripple suppression control. This suggests that the torque ripple suppression control increases copper loss even during variable speed drive.

3.3.2. Electricity consumption evaluation

Here, the electricity consumption with and without torque ripple suppression control is calculated. Note that electricity consumption [km/kWh] is defined as the distance [km] that can be driven per 1 kWh, taking into account both energy used during driving and energy recovered through regenerative braking. The electricity consumption with and without torque ripple suppression control are 7.64 km/kWh and 7.65 km/kWh, respectively. This indicates that total loss is increased with torque ripple suppression control considering magnetic saturation; however, the increase is small and does not significantly affect to electricity consumption. Hence, by applying this control to EVs, torque ripple can be suppressed with a small increase in a total loss, which is unlikely to have a significant influence on electricity consumption.

4. CONCLUSION

This paper verified the influence of the control method that can suppress torque ripple under a wide operating range on loss and electricity consumption. Total efficiency with torque ripple suppression control declines in almost all operating ranges compared to

without torque ripple suppression control. Furthermore, variable speed drive using the urban driving phase of the WLTC driving mode was conducted, and the influence of the torque ripple suppression control considering magnetic saturation was verified. The results show that the increase of total loss under variable speed drive with torque ripple suppression control is approximately 2 kJ, and this increase is 0.2% compared to without ripple suppression control. Hence, the torque ripple suppression control considering magnetic saturation can suppress torque ripple with a small reduction in electricity consumption.

ACKNOWLEDGMENT

This research was commissioned by Transmission Research Association for Mobility Innovation (TRAMI) in FY2022 and was conducted using the equipment of the open laboratory at Japan Automobile Research Institute (JARI). We would like to express our gratitude to all those involved.

References

(1) Y.Tadano, T.Akiyama, M.Nomura, M.Ishida: "Torque Ripple Suppression Control Based on the Periodic Disturbance Observer with a Complex Vector Representation for Permanent Magnet Synchronous Motors", *IEEJ Trans.on IA*, vol. 132, no. 1, pp. 84-93 (2012) (in Japanese)

(2) N.Nakao, K.Akatsu: "Suppressing Pulsating Torques: Torque Ripple Control for Synchronous Motors", *IEEE Industry Applications Magazine*, vol. 20, no. 6, pp. 33-44 (2014)

(3) Y.Terayama, N.Hoshi: "A Study on Torque Ripple Suppression for Permanent Magnet Synchronous Motor using Estimated Harmonic Components of Linkage Flux at High Speed Rotation", *Annual Meeting Record IEEJ*, 5-094 (2020) (in Japanese)

(4) S.Nakata, N.Hoshi, T.Yamaguchi: "A novel suppression method of 6th-order torque ripple of permanent magnet synchronous motor without torque meter", *Proc. of International Conference on Electrical Machines and Systems(ICEMS)*, Pattaya, Thailand, pp. 1479-1485 (2015)

(5) H.Hida, Y.Tomigashi, K.Ueyama, Y.Inoue, S.Morimoto: "New Torque Estimation Method Considering Spatial Harmonics and Torque Ripple Reduction in Permanent Magnet Synchronous Motors", *IEEJ Trans. on IA*, vol. 130, no. 9, pp. 1051-1058 (2010) (in Japanese)

(6) N.Nakao, K.Tobari, T.Sugino, Y.Ito, M.Mishima, D.Maeda: "Torque Ripple Suppression Control for PMSMs using Feedforward Compensation and Online Parameter Estimation", *IEEJ Transactions on Industry Applications*, vol. 141, no. 1, pp. 18-27 (2021) (in Japanese)

(7) Y.Terayama, N.Hoshi: "Torque Ripple Suppression Control in PMSM Using Estimated Harmonic Component of Flux Linkage Considering Magnetic Saturation", *IEEJ Transactions on Industry Applications*, vol. 141, no. 4, pp. 366-373 (2021) (in Japanese)

(8) N.Nakao, K.Akatsu: "Torque Ripple Suppression of Permanent Magnet Synchronous Motors Considering Total Loss Reduction", *Proc. of IEEE Energy Conversion Congress and Exposition, Denver, CO*, pp. 3880-3887 (2013)

(9) K.Kawarazaki, N.Hoshi, "Torque Ripple Suppression Control for Interior Permanent Magnet Synchronous Motor Considering Nonlinearity of Magnetic Saturation and Variation of Magnetization Characteristics on Temperature", *Mar.2023 Joint Technical Meeting on Motor Drive/Home and Consumer Appliances*, MD-23-060/HCA-23-004, pp. 17-22 (2023) (in Japanese)

(10) K.Honda, K.Akatsu: "Driving an Open-Winding Structure PMSM Using Third Harmonic Current Control", *IEEJ Transactions on Industry Applications*, vol. 141, no. 1, pp. 39-45 (2021) (in Japanese)